Tampereen yliopisto
Tampere University

Leevi Kallioniemi

THREE-DIMENSIONAL SECOND-HARMONIC GENERATION MICROSCOPY OF SEMICONDUCTOR NANOWIRES USING TAILORED FOCAL FIELDS

Bachelor of Science Thesis

Examiners: Dr. Godofredo Bautista and Prof. Martti Kauranen

May 2019

ABSTRACT

LEEVI KALLIONIEMI: Three-Dimensional Second-Harmonic Generation Microscopy of Semiconductor Nanowires using Tailored Focal Fields
Tampere University
Bachelor of Science Thesis, 27 pages
May 2019
Bachelor's Degree Programme in Science and Engineering
Major: Engineering Physics
Examiners: Dr. Godofredo Bautista and Prof. Martti Kauranen
Keywords: Second-Harmonic Generation, Three-Dimensional Microscopy, Semiconductor Nanowire, Polarization, Longitudinal Electric Field

Nonlinear optical (NLO) microscopy has raised much interest with its superior capabilities in high-resolution imaging of a variety of nanostructures without photodamage or labeling. Contrast in NLO microscopy relies on NLO effects, which are sensitive to the crystal structure and the physical properties of the sample at nanoscale. It turns out that the polarization of the input electromagnetic field also matters in the improvement of image contrast. In the context of NLO microscopy, it is evident that the capability to control the polarization in three dimensions at the beam focus is important. Such capability is important in the characterization and exploitation of individual nanostructures with well-known or even unexplored NLO properties. The goal of this Thesis was to perform SHG microscopy of individual vertically-aligned GaAs nanowires in three dimensions. Previously, such kind of nanowires was found to be very sensitive to the electric field component along the beam propagation axis, which can be taken advantage of when mapping the longitudinal electric field distribution of the beam. We also present a method to redistribute the longitudinal electric field of a tightly focused first-order Hermite-Gaussian (HG_{10}) beam by spatially phase-shaping the beam. By using the presented techniques, the longitudinal electric field distribution of a spatially phase-shaped HG_{10} beam was verified for the first time in three dimensions.

PREFACE

The work of this thesis was performed in the Nonlinear Optics research group of the Laboratory of Photonics at Tampere University. The experimental work was carried out during summer 2018. The experiments and the writing of this thesis was done under supervision of Dr. Godofredo Bautista and Prof. Martti Kauranen.

First of all, I would like to thank my examiner Godo for his guidance and feedback for this thesis and during the whole time I have worked at the lab. Secondly, I would like to thank collaborators at Aalto University for providing the samples for the experiments. For the great working environment, I would like to thank all the people in the Photonics lab. Especially I'd like to thank Leo for helping and guiding in the practical work and answering questions, and Timo for giving valuable feedback on my thesis.

Finally, I would like to thank my family and all of my friends for all the fun in life and motivation to keep going.

Tampere, 5.4.2019
Leevi Kallioniemi

CONTENTS

LIST OF ABBREVIATIONS AND SYMBOLS

GaAs	Gallium arsenide
CVB	Cylindrical vector beam
HG	Hermite-Gaussian
LP	Linearly polarized
LCD	Liquid-crystal display
NW	Nanowire
NLO	Nonlinear optics
PMT	Photomultiplier tube
SEM	Scanning electron microscope
SHG	Second-harmonic generation
SOP	State of polarization
3D	Three-dimensional
TEM	Transverse electromagnetic mode

ω	Angular frequency
w	Beam waist
x, y, z	Cartesian coordinates
c.c.	Complex conjugate
$\mathbf{E}(\mathbf{r}, t)$	Electric field
$E_{\|\|}$	Electric field along a nanowire axis
$u_{l,m}$	Electric field of a HG beam
$E_{\perp}$	Electric field perpendicular to a nanowire axis
w_0	Incident beam waist size
$\mathbf{r}$	Location vector
$\mathbf{P}(t)$	Material polarization
$\mathbf{P}^n(t)$	Material polarization of n:th order
l, m	Order of a HG beam
R	Radius of the curvature
$u(x, y, z)$	Scalar electric field amplitude
$\chi^{(n)}$	Susceptibility of n:th order
t	Time
$\mathbf{k}$	Wave vector

1. INTRODUCTION

Optics plays a major part in many of our everyday technologies. Understanding light and its interaction with matter is nowadays needed everywhere and has many applications. Probably the most important properties of light are wavelength, intensity and polarization. Of these, polarization is not so evident in our everyday world, as it can not be perceived with the naked eye. As will be seen in this Thesis, polarization is a very important property as the vectorial nature of light gives rise to many interesting phenomena. Especially at nanoscale, studying how polarization of light affects the light-matter interactions can provide much useful information.

Nonlinear optics is a study of optical processes which require high intensity illumination [1]. For instance, focusing a high power laser beam onto certain materials can give rise to a process called second-harmonic generation (SHG). In SHG, two incident photons hit the material and combine into one photon with double the original frequency. Along with many other factors, this process is very sensitive to the polarization of the incident field. The sensitivity of SHG and other nonlinear processes is used in nonlinear optical (NLO) microscopy to study objects by observing how the physical structure of the sample interacts with polarization of the incident field [2]. NLO microscopy can be used to study artificial or man-made samples (e.g., semiconductor, dielectric, metal, etc.) and biological samples (e.g. collagen, cell, biotissue, lipids) [3, 4, 5].

The ability to probe light with nano-objects in general can be used in optical trapping and many other applications. This raises a demand for the capability to control different polarization components of a laser beam. A three-dimensional (3D) polarization distribution can be created by tightly focusing light [2, 6, 7]. In laser beams that are polarized in a certain way, a longitudinal (along the direction of light propagation) polarization component is also created. By manipulating the polarization of the incident beam, the properties of the longitudinal field at the focus can be manipulated. In many cases, the need for manipulation leads to very cumbersome solutions where the optical setup has to be physically modified to alter the beam polarization.

In addition to the control of the electric field at the beam focus, it is important to know the actual field distribution that is generated. Thus, reliable verification methods are needed. It is a well-known fact that SHG from vertically aligned semiconductor nanowires is sensitive to longitudinal polarization component [8]. Therefore, nanowires can be used to probe the longitudinal field in order to map the beam polarization distribution. This Thesis aims to provide a more flexible way to control and verify the longitudinal electric field distribution in three dimensions with spatial light shaping. With the used methods one can easily have control over the longitudinal field without touching the actual optical components.

This Thesis consists of five chapters. The first chapter is this introduction and the second one provides more in-depth background theory. In the third chapter, the experimental setup is introduced and the experimental results are described in Chapter 4. The fifth chapter, being the last, draws conclusions of this study and provides a future outlook of the work.

2. OPTICS

Optics is a subfield of physics that studies light. Light can be treated as massless particles called photons or as wave motion of the electromagnetic field. The appropriate approach depends on which optical phenomenon is described. Electromagnetic wave motion has an electric and a magnetic component which oscillate perpendicular to each other. Usually in optics, the electric field component is the one that raises interest.

The electric component of an electromagnetic plane wave can be represented mathematically in the form

$$\mathbf{E}(\mathbf{r}, t) = \mathbf{E}_0 e^{i(\mathbf{k}\cdot\mathbf{r}-\omega t)} \tag{2.1}$$

where $\mathbf{E}_0$ is the amplitude of the electric field, $\mathbf{k}$ is the wave vector, $\mathbf{r}$ is the position vector, ω is the angular frequency, and t is time. This field is complex valued and the actual real-valued field is the real part of Equation 2.1, but often calculations are easier using the complex form. The direction in which the field oscillates is related to the vector-valued amplitude $\mathbf{E}_0$. It can be represented as

$$\mathbf{E}_0 = \hat{\mathbf{p}} E_0 \tag{2.2}$$

where E_0 is the scalar amplitude and $\hat{\mathbf{p}}$ is a unit vector in the direction of oscillation, also referred to as polarization. The vectorial nature of light is an important factor in many linear optical [9], and NLO phenomena [2].

The interaction of light and matter can be described with material polarization. Polarization of a medium is not to be confused with the polarization of light mentioned above. The polarization field is induced when the incoming electric field excites the material. It has a linear connection to the original electric field:

$$\mathbf{P}(t) = \epsilon_0 \chi^{(1)} \mathbf{E}(t) \tag{2.3}$$

where ϵ_0 is the permittivity of vacuum, $\chi^{(1)}$ is the linear susceptibility, and $\mathbf{E}(t)$ is the incident electric field exciting the material. Here, the susceptibity χ is a tensor, but due to isotropy or high symmetry it can be assumed as scalar.

2.1 States of Polarization

Light wavefronts with different polarization and intensity distributions are called modes. Transverse electromagnetic modes (TEM) are mathematically derived by assuming that the electric field oscillates purely in the transverse direction compared to beam propagation. The direction of oscillation is always uniformly the same across the whole wavefront.

To generate NLO effects, which will be discussed later, one must have very strong electric fields. As a solution, use of lasers is a common way to generate NLO effects. The output of a laser is a superposition of fundamental and higher-order TEMs. It is usually desirable that lasers emit only the lowest order mode. This is the so-called Gaussian beam as the intensity distribution follows the Gaussian curve. The Gaussian beam profile is the most commonly used and studied beam in optics.

2.1.1 Transverse Electromagnetic Modes

A propagating laser beam can be mathematically described with transverse electromagnetic modes. The mathematical form of the beam has to fulfill the boundary conditions for the system and be a solution to the paraxial wave equation [10, p. 149]

$$\nabla^2 u - 2ik\frac{\partial u}{\partial z} = 0 \tag{2.4}$$

so that the solution retains its functional form. Here, k is the wave number, z is the direction of propagation, and u is a scalar mode function. A particular set of solutions for this are the Hermite-Gaussian (HG) beams which are modes generated in a system that has rectangular symmetry.

Let us assume that a HG beam of orders l and m is propagating in the positive z-direction. Now, the scalar electric field amplitude $u(x, y, z)$ is [10, p. 158]

$$u_{l,m}(x,y,z) = \frac{w}{w_0} H_l\left(\frac{\sqrt{2}x}{w}\right) H_m\left(\frac{\sqrt{2}y}{w}\right) exp\left(-\frac{x^2+y^2}{w^2}\right) exp\left(-i\frac{k(x^2+y^2)}{2R} + i(1+l+m)\phi\right) \tag{2.5}$$

where x and y are the Cartesian coordinates in transverse direction. The waist w determines the spot size of the beam, and the radius of the curvature R tells how fast the beam is diverging/converging. They are defined by equations [10, p. 153]

$$w^2(z) = w_0^2\left[1 + \left(\frac{\lambda z}{\pi w_0^2}\right)^2\right] \tag{2.6}$$

$$R(z) = z\left[1 + \left(\frac{\pi w_0^2}{\lambda z}\right)^2\right] \tag{2.7}$$

where w_0 is the beam waist at its smallest. Function H_j is a Hermite polynomial of order j. With the lowest order mode TEM_{00} (or HG_{00}), the zeroth-order Hermite polynomial has a the value of 1, and the intensity distribution follows a Gaussian distribution.

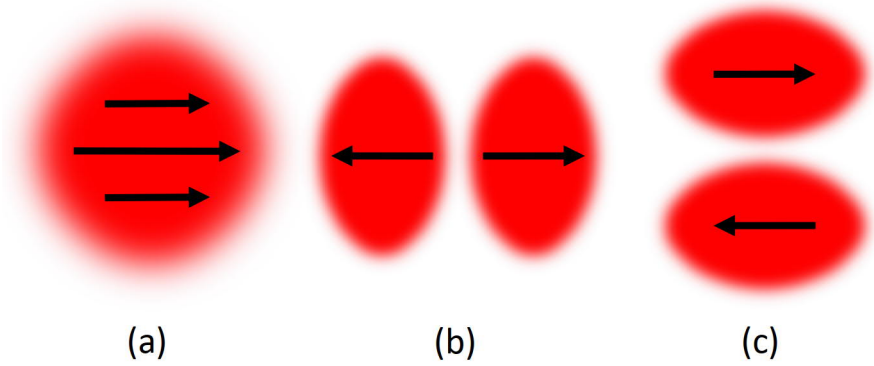

Figure 2.1 *Schematics of intensity patterns and polarization states of a linearly polarized (a) Gaussian beam, (b) HG_{10} beam, and (c) HG_{01} beam. The arrows represent the state of polarization at a certain instant.*

The lowest order mode seen in Figure 2.1(a) is called linearly-polarized (LP) Gaussian beam. The second-order mode HG_{10} has the intensity distribution of two lobes seen in Figure 2.1(b). If the l and m are interchanged, the intensity pattern stays identical but is rotated by 90°. The phase of the two lobes differs by π which is

equal to the polarization being flipped in plane to the opposite direction.

2.1.2 Cylindrical Vector Beams

By combining TEM modes of different orders in various ways, beams with spatially varying states of polarization (SOPs) can be synthesized. Cylindrical vector beams (CVBs) are popular examples of such beams. Radial and azimuthal polarizations are the most commonly used and studied CVBs. Radially polarized CVB is a superposition of two orthogonal HG_{10} modes, and the electric field oscillates in the radial direction in every part of the beam. Azimuthally polarized CVB consists of two HG_{01} modes, and the electric field oscillates in the tangential direction of the beam. Their intensity pattern is doughnut-shaped as seen in Figure 2.2.

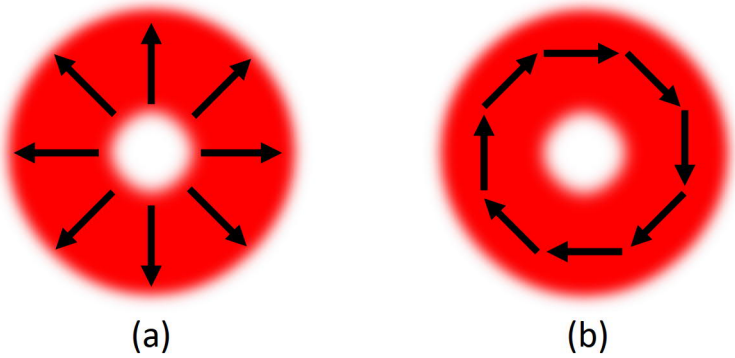

Figure 2.2 *(a) Radially polarized CVB. (b) Azimuthally polarized CVB. The arrows indicate the direction of local linear states of polarizations.*

CVBs have many interesting properties [9]. In the context of this work and nonlinear optical (NLO) microscopy, the focal field distributions of CVBs are even more important [2].

2.1.3 Focal Fields

In Subsection 2.1.1, the polarization of the beam was purely in the transverse direction. However, when the beam is tightly focused, this description is not valid anymore as it was derived using a paraxial approximation [11]. Under tight-focusing conditions, even unpolarized light shows vectorial nature in the focal volume [7]. Furthermore, 3D polarization distribution is achieved already by tightly focusing a LP beam. In this case, a polarization component in the direction of the beam propagation is created [6]. This is referred to as longitudinal electric-field component. 3D vector fields in the focal volume of a tightly focused laser beam have many

useful applications, for example, in optical trapping, electron acceleration and NLO microscopy [2, 12, 13, 14].

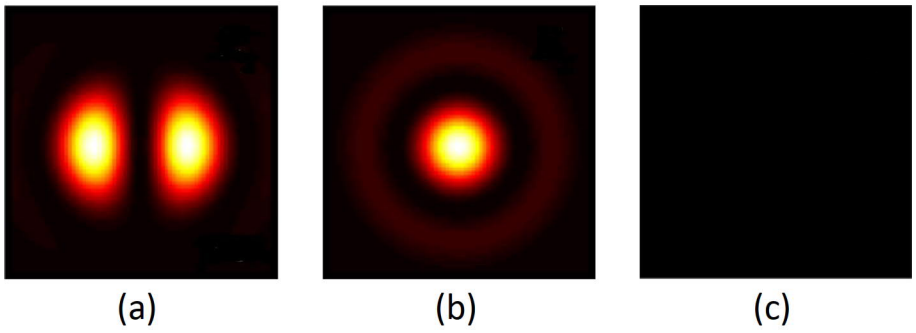

Figure 2.3 *Intensity distributions of the longitudinal electric field component of (a) a linearly polarized Gaussian beam polarized along horizontal axis, (b) radially polarized CVB and (c) azimuthally polarized CVB. Adapted with permission from reference [2].*

Spatial intensities of the longitudinal electric-field components of focused beams are shown in Figure 2.3. The intensity distributions are in transverse direction compared to the beam propagation. The longitudinal electric field of a focused LP beam shows a two-lobed intensity distribution. Focused radially polarized CVB shows a spot-like intensity distribution located along the axis of beam propagation. Azimuthally polarized CVB has no longitudinal field component in the focal volume. The intensity of the generated longitudinal electric-field depends on the numerical aperture of the used objective, but in these examples, the focused radially polarized CVB has the most intense longitudinal field component, larger by a factor of 100 compared to the linearly polarized beam.

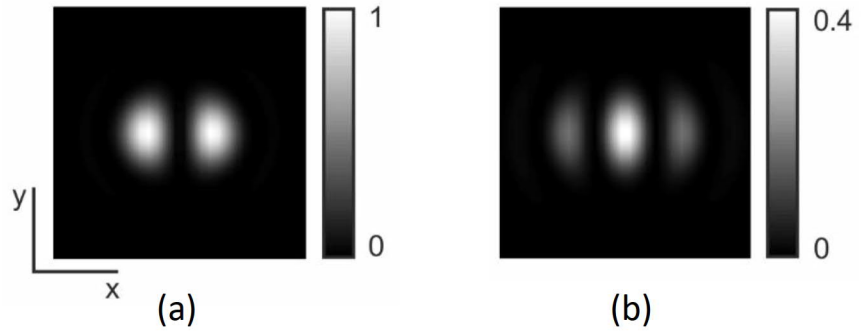

Figure 2.4 *Intensity distributions of the (a) transversal and (b) longitudinal electric fields of a tightly focused HG_{10} beam. The incident HG_{10} is polarized along x. Adapted from [15, Figure S2].*

The focusing properties of HG_{10} beam can be seen in Figure 2.4. Subfigure 2.4(b) shows the longitudinal field in the transverse direction, which in this case has a three-lobe distribution where the middle lobe has the strongest intensity. The patterns in Figures 2.3 and 2.4 are theoretically calculated, but can also be verified experimentally, which will be done later in this Thesis.

2.2 Nonlinear Optics

Earlier, the material response to the electric field was assumed to be linear. When the electric field is strong enough, higher-order terms in the material polarization become significant. In this case, the material polarization can be described using the power series [1, p. 2]:

$$\tilde{\mathbf{P}}(t) = \epsilon_0\chi^{(1)}\tilde{\mathbf{E}}(t) + \epsilon_0\chi^{(2)}\tilde{\mathbf{E}}^2(t) + ... + \epsilon_0\chi^{(n)}\tilde{\mathbf{E}}^n(t) = \tilde{\mathbf{P}}^1(t) + \tilde{\mathbf{P}}^2(t) + ... + \tilde{\mathbf{P}}^n(t) \quad (2.8)$$

where $\chi^{(n)}$ is the susceptibility of the n:th order, and $\mathbf{P}^n(t)$ is the polarization term of the n:th order. The susceptibilities $\chi^{(n)}$ are tensors and the tilde $\sim$ means that the quantity is rapidly oscillating in time. As can be seen below, the nonlinear terms in the material polarization may allow generation of electric fields at different frequencies. The real-valued time-dependent incident electric field $\tilde{\mathbf{E}}(t)$ is defined to be

$$\tilde{\mathbf{E}}(t) = \mathbf{E}e^{-i\omega t} + \mathbf{E}^* e^{i\omega t} = \mathbf{E}e^{-i\omega t} + c.c. \quad (2.9)$$

where *c.c.* stands for the complex conjugate. In this work, the focus is on the phenomena that occur from the second-order polarization term and especially on the second-harmonic generation (SHG). SHG is a process in which two photons excite an atom into a virtual state, and the atom emits one photon with doubled frequency. The process is parametric which means that the interacting atom itself is not excited, and therefore no energy absorption to the material occurs in SHG. The photon diagram of SHG is shown in Figure 2.5.

According to Equation 2.8, the second-order polarization can be written as

$$\tilde{\mathbf{P}}^2(t) = \epsilon_0\chi^{(2)}\tilde{\mathbf{E}}^2(t) \quad (2.10)$$

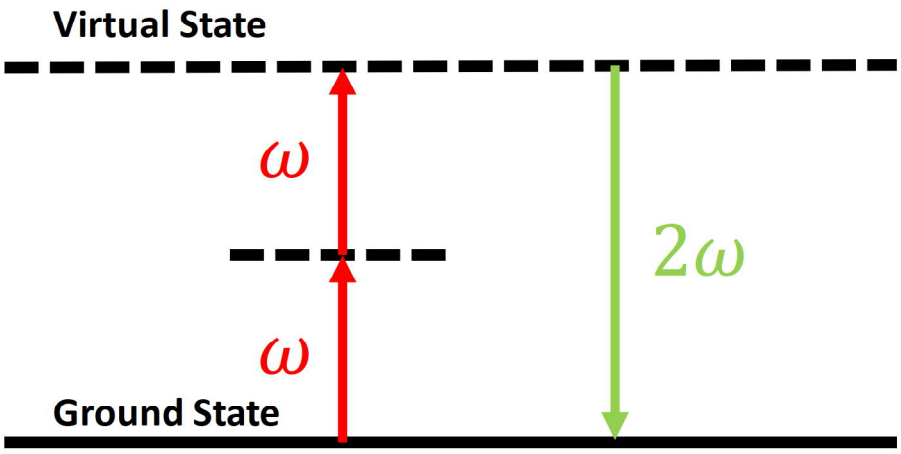

Figure 2.5 *Photon diagram of SHG*

and by substituting Equation 2.9 into Equation 2.10 we get

$$\tilde{\mathbf{P}}^2(t) = \epsilon_0 \chi^{(2)} (\mathbf{E} e^{-i\omega t} + c.c.)^2 \tag{2.11}$$

from which we can derive

$$\tilde{\mathbf{P}}^2(t) = 2\epsilon_0 \chi^{(2)} |\mathbf{E}|^2 + \epsilon_0 \chi^{(2)} (\mathbf{E}^2 e^{-2i\omega t} + c.c.) \tag{2.12}$$

The first term of Equation 2.12 is a constant in time which indicates that the second-order nonlinear process gives rise to a constant electric field in the nonlinear material. This phenomenon is called optical rectification. The second term is the oscillating part of the induced polarization field. The oscillation frequency has now doubled compared to the incident field.

SHG is generally sensitive to the symmetry of the material. It can be shown that all the even-order susceptibilities $\chi^{(2n)}$ vanish for centrosymmetric media [1, p. 42]. This means that SHG can happen in only certain materials that have noncentrosymmetric crystal structure. Similarly, SHG can be generated at interfaces where the symmetry is broken. The generation of SHG is also dependent on how the SOP of the incident field couples with the physical properties of the sample. Usually, a component in the direction of the normal of the surface needs to be present to generate SHG. [2]

2.3 Second-Harmonic Generation Microscopy

The high selectivity makes SHG a great source of contrast in imaging a variety of materials as well as nano-objects. As discussed in Subsection 2.1.3, strong focusing of the incident electric field produces a 3D polarization distribution which can be used to probe the sample. This provides plenty of useful information about the sample in higher resolution compared to the traditional optical microscopy, as the interaction volume of SHG is highly localized [16]. Another advantage of SHG is that no energy is transferred between the photons and the material, thus allowing imaging without photodamage.

The SHG response of different nano-objects has already been studied in NLO microscopy. For relatively thin semiconductor nanowires (NWs), the electric field $\mathbf{E}$ inside the NW can be written as [17]

$$E_{||} = E_{0||} \tag{2.13}$$

$$E_{\perp} = \frac{2\varepsilon_0 E_{0\perp}}{\varepsilon_0 + \varepsilon} \tag{2.14}$$

where $E_{||}$ is the field component parallel to the NW, and $E_{\perp}$ is component perpendicular to the NW. The $E_{0||}$ and $E_{0\perp}$ are the corresponding components of the incident electric field $\mathbf{E}_0$. The quantities ε and ε_0 are the dielectric constants of the NW and the medium surrounding the NW, respectively. As can be seen from Equation 2.14, if $\varepsilon \gg \varepsilon_0$, the electric field perpendicular to the NWs is greatly suppressed. This means that the induced polarization field, hence the SHG response of the NW, is mainly from the polarization component along the NW axis. [17]

Semiconductor NWs have also been experimentally studied by NLO microscopy, and their SHG response is well-known and in agreement with theoretical results. Vertically aligned gallium arsenide (GaAs) nanowires respond mainly to the longitudinal component of the incident electric field [8]. One can take advantage of the well-known SHG response of GaAs NWs in the verification of known and unknown longitudinal field distributions in the focal volume of the NLO microscope beam.

3. METHODOLOGY

The microscopy and phase-shaping setup used in the experiments will be discussed in this chapter. After that, the samples used in the work to verify longitudinal electric fields experimentally are presented.

3.1 NLO Microscopy Setup

The measurements used in this Thesis were acquired using a custom-built NLO microscopy setup. The schematic of the setup is shown in Figure 3.1. Briefly, a femtosecond laser (wavelength of 1060 nm, pulse length of 140 fs, repetition rate of 80 MHz) was used as the excitation source of our NLO microscope. Our setup utilized a computer-controlled stage-scanner for moving the sample in relation to the focused beam. The sample scanning approach was used in order to avoid unexpected polarization scrambling effects that are inherent to beam scanning systems. To focus the laser beam, a high numerical aperture microscope objective (Nikon CFI LU Plan Fluor Epi P, numerical aperture of 0.8 50X N.A. 0.80/W.D. 1.0mm, infinity corrected, semi-apochromat, 50x magnification) was used, and the back-reflected nonlinear signal was collected by the same objective, and then directed to a cooled photomultipler tube.

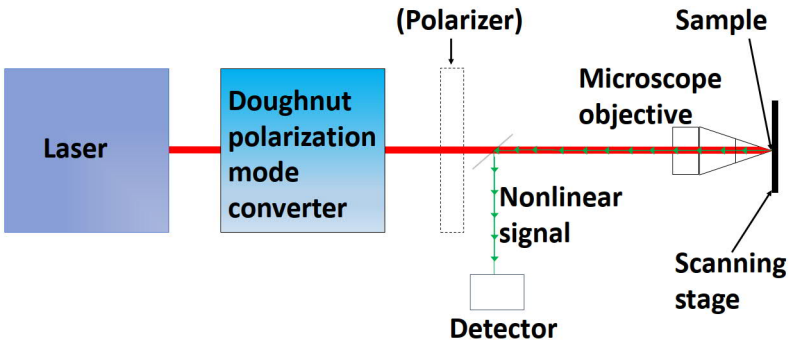

Figure 3.1 *Schematic of the NLO microscope*

Our microscope allows the possibility to easily switch between various beam polarizations (e.g., linear, radial and azimuthal) and shapes (e.g., HG modes, Bessel and petal). Using a commercial doughnut polarization mode converter (e.g., Arcoptix), a linearly polarized beam can be converted into a CVB with radial or azimuthal polarization. To achieve HG_{10} mode, a polarizer can be put in front of the radially polarized CVB. Intensity profiles of the radially polarized CVB before and after the polarizer can be seen in Figure 3.2. The polarization mode converter can be bypassed, if the desired output is a LP beam. After the desired beam shape is achieved, the beam is focused onto the sample mounted on a piezo-scanning stage. In the last stage, collecting and properly filtering the back-reflected nonlinear signal takes place.

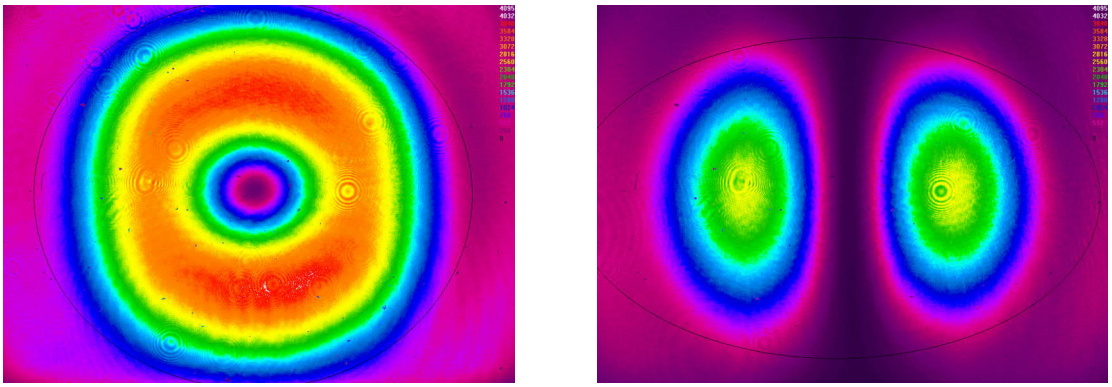

(a) (b)

Figure 3.2 *The beam profile of a radially polarized CVB (a) before, and (b) after the polarizer. The polarizer axis direction is horizontal.*

The average power of the laser beam in front of the objective was controlled with a half-wave plate and a polarizing beamsplitter. Excitation power of 1 mW was used in all the experiments performed in this work. A LabVIEW-program was used to operate the stage-scanner and collect data to perform a scan. In the software, the user can decide various parameters for the scan, of which the scan area and pixel resolution are the most important. The program collects the nonlinear signal from each pixel one at a time from the scan area. The signal collection time at each pixel can be determined. In our experiments, the collection time was 50 ms and the measured nonlinear signal was SHG. An example scan of an array of vertically-aligned GaAs nanowires (see Section 3.3) can be seen in Figure 3.3.

The scan area of the measurement in Figure 3.3 is $10 \times 10 \mu$m and the pixel resolution is $0.1 \mu m$. With these parameters the scan time is approximately 13 minutes. The scan was taken along the xy-plane using a radially polarized CVB. The nanowires are seen as dots which correspond to the longitudinal electric field distribution of

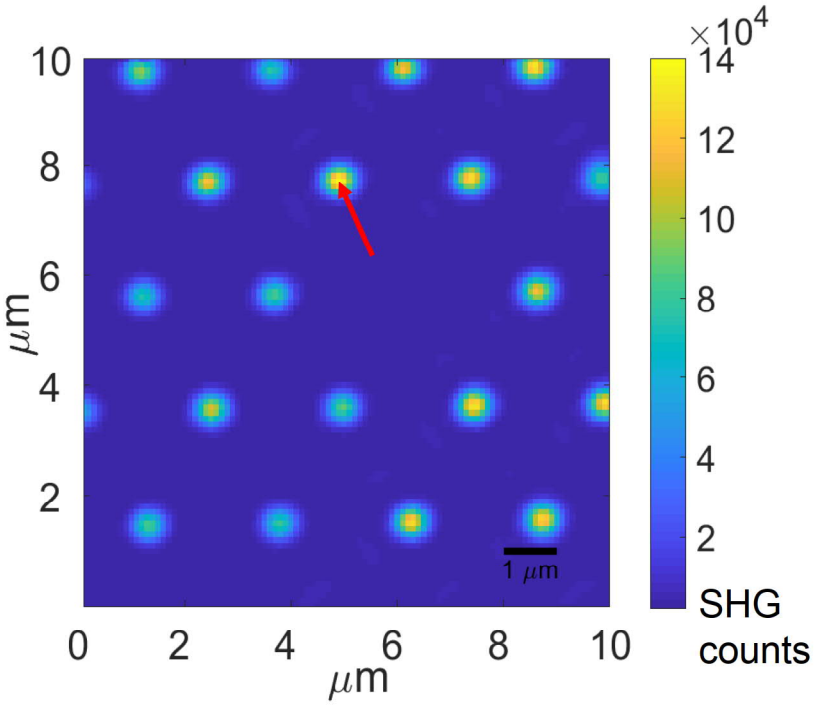

Figure 3.3 *An example scan of periodically- arranged vertically-aligned GaAs nanowires on GaAs substrate. with the NLO microscope using a radially polarized CVB.*

the used beam profile. The maximum detector counts was roughly 140 000 which is relatively high, as the longitudinal electric field of a focused radially polarized CVB is quite strong [8, 18]. A defect in the nanowire array can be seen in the middle of the picture. These are good points of reference when comparing consequent scans as there is always minor movement of the sample between the scans.

3.2 Phase-Shaping Techniques

To control the longitudinal electric-field distribution of a focused beam, one must be able to modify the incident beam entering the microscope objective. For this Thesis, we relied on phase-shaping techniques using a spatial light modulator (SLM). This approach was chosen because of its inherent flexibility, which is not provided by traditional and physical diffracting optical elements (e.g., axicon, kinoform, lenslet arrays and so on). The SLM is a pixelated device that lets the user assign an individual phase or amplitude or both to each pixel. In this way, the incident beam can be controlled spatially by creating arbitrary diffraction patterns. The phase distribution of the SLM can be computer-calculated from the desired pattern in the output plane.

SLMs are widely used in various applications. They can be used, for example, to

generate CVBs [19, 20, 21], control optical tweezers [22], or even to generate arbitrary hologram patterns [23]. In this work we used a phase-reflective Hamamatsu LCOS-SLM with a pixel resolution of 792×600. The schematic of the phase-shaping setup is seen in Figure 3.4.

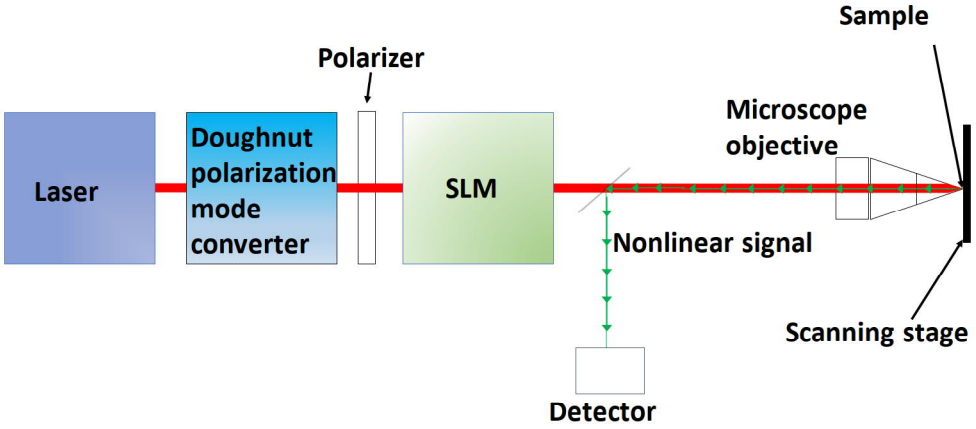

Figure 3.4 *Schematic of the NLO microscope including the phase-reflective Hamamatsu LCOS-SLM.*

The principle of SLM is based on liquid-crystal display (LCD) whose orientation is controlled individually in each pixel. The SLM is controlled by creating gray level maps with values between 0 and 255. The value of each pixel corresponds to an additional phase delay provided by the SLM. The phase delay that the light beam is experiencing depends on the used wavelength, but in our setup (with a wavelength of 1060 nm) the maximum gray value of 255 corresponds to a phase delay of 2π.

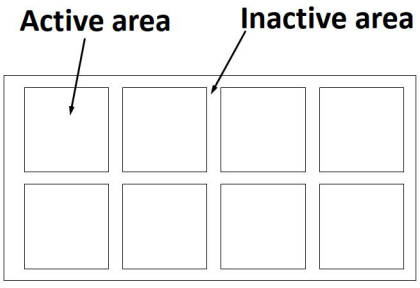

Figure 3.5 *The pixelated structure of SLM with nonunity fill factor, showing the active area and inactive space between pixels*

However, the real phase response curve could be slightly nonlinear between 0 and

256, corresponding 0 and 2π delays, respectively. This means that a linear phase-ramp is actually curved if the nonlinearity is not taken into account. Another factor causing artefacts comes from the physical layout of the pixels of the SLM with non-unity fill factor. As illustrated in Figure 3.5, the pixels are not located right next to each other but there is always space between the pixels where the phase can not be controlled. Therefore a part of the incident beam always remains undiffracted which is referred to as a zeroth-order beam. The percentage of the active area of the SLM window is referred to as fill factor, which for our SLM was 98 %. Due to the relatively high fill factor, the zeroth order beam should not be a major issue in our setup.

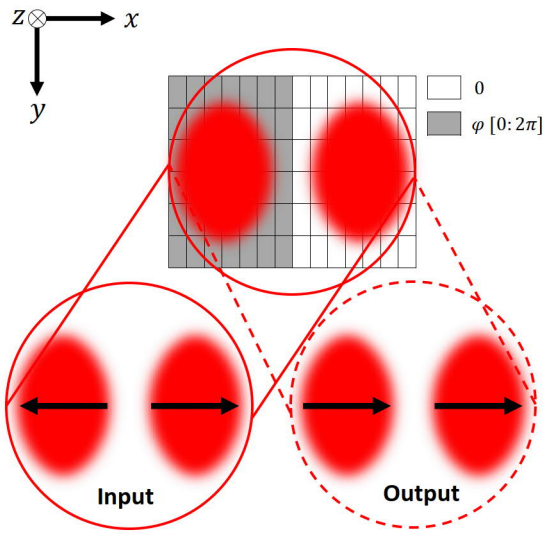

Figure 3.6 *The phase shaping scheme to control the spatial distribution and strength of longitudinal electric fields. The phase delay φ varies between 0 and 2π.*

Our SLM works only for x-polarized light, so a HG_{10} mode polarized in the x-direction was used as a basis of the phase-shaping experiments. It is a well-suited option for the purposes of this work as it shows a strong longitudinal electric field component when tightly focused. This has also been used as a reliable basis of previous demonstrations of manipulating longitudinal electric fields in the focal volume [15, 24, 25, 26].

In the phase shaping experiment, the SLM window was divided in half, and the HG_{10} mode was directed so that each lobe reflects from a different subwindow. This is shown in Figure 3.6. Now a global phase delay can be applied onto each lobe separately. The phase delay of one window was kept at 0 as the phase delay of the other window was gradually increased from 0 to 2π. [15]

3.3 Sample

The longitudinal electric field distribution at the focus was studied by scanning straight-standing GaAs nanowires on a GaAs substrate. As was discussed in Section 2.3, their SHG response is well-known. They respond mainly to the longitudinal electric field component which made them ideal probes for our purposes. The NWs were fabricated at Aalto University by the research group of Harri Lipsanen. Scanning electron microscope (SEM) images of the NWs are shown in Figure 3.7.

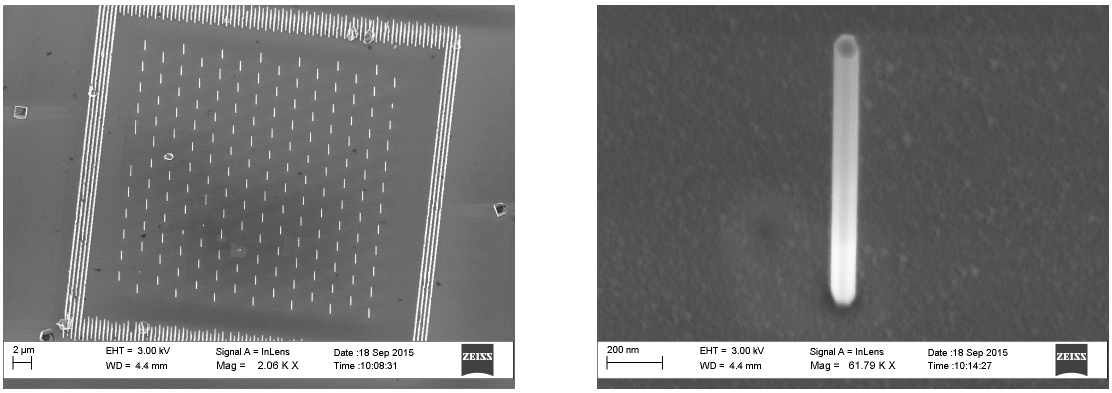

(a) (b)

Figure 3.7 *SEM images of (a) periodic structure of the vertically-aligned GaAs nanowires (b) an individual nanowire.*

Selective-area metallo-organic vapour-phase epitaxy (SA-MOVPE) was used to fabricate the NWs. Shortly, the GaAs substrate is covered with a silicon oxide layer of 40 nm. Periodic holes are made to the silicon oxide layer. The substrate is exposed to a vapor precursor containing Ga and As atoms, and the growth happens atom-by-atom from the holes in the silicon oxide layer. The growth can happen only in the growth direction of the substrate, so a straight standing structure is acquired.

NWs with different period and thickness can be constructed by controlling the period and diameter of the holes in the silicon oxide layer. In this work, a period of 2.5 μm and a diameter of 55 nm was used for probing the longitudinal electric field distribution. The period was chosen to be relatively high to avoid coupling effects between the nanowires so that the signal would always be coming from an individual nanowire. The length of the nanowires was from 2 to 2.5 μm on average. [27, p. 47]

4. RESULTS

This chapter will cover the experimental work that was done for the Thesis. The microscope images were taken from an area of 10×10 μm with a pixel resolution of 0.1 μm. The raw data that was acquired using the microscope was plotted with Matlab. First, routine experiments were made to verify the longitudinal electric field distributions of the reference LP, RP, AP and HG_{10} beams. After that, the results of the phase shaping experiment of Section 3.2 are shown.

4.1 Reference Beams

The longitudinal electric field distributions of the different vector beams were verified first using the SHG microscopy of a single GaAs nanowire in 3D. As was discussed in the earlier chapters, the verification was done by scanning individual vertically-aligned GaAs nanowires within the focal volume of interest. The schematic diagram of the scanning plane relative to the nanowire is shown in Fig. 4.1.

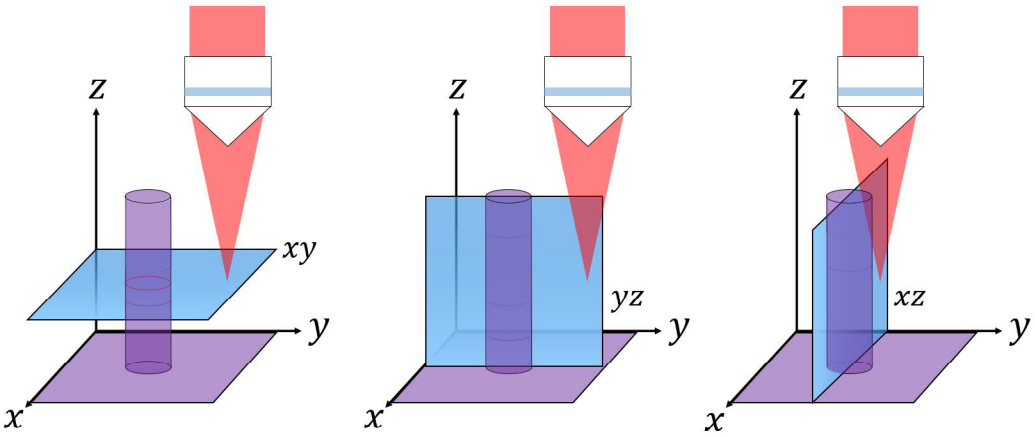

Figure 4.1 *Different scanning planes used to map the SHG intensities in three dimensions. The figures show the orientation of the planes relative to the nanowire.*

The scanning SHG maps taken using the reference vector beams are shown in Figure 4.2. As can be seen, the SHG maps from the nanowire mimics, to some extent,

the qualitative features of the theoretical intensity distributions of the longitudinal electric fields of the corresponding focused beam. The SHG-response of the nanowire shows a two-lobe distribution when a LP beam is used. The direction of the lobes is related to the SOP of the input beam. In this case, the SOP is oriented along the y-axis of the microscope coordinates, hence the lobes are also oriented along the y-axis. Compared to the background, the signal level is also low when the nanowire is symmetrically illuminated by the LP beam, i.e., the in-plane positions of the beam center and nanowire coincide. This is because at the center of the beam, there is no longitudinal electric field component that could drive the SHG response of the nanowire.

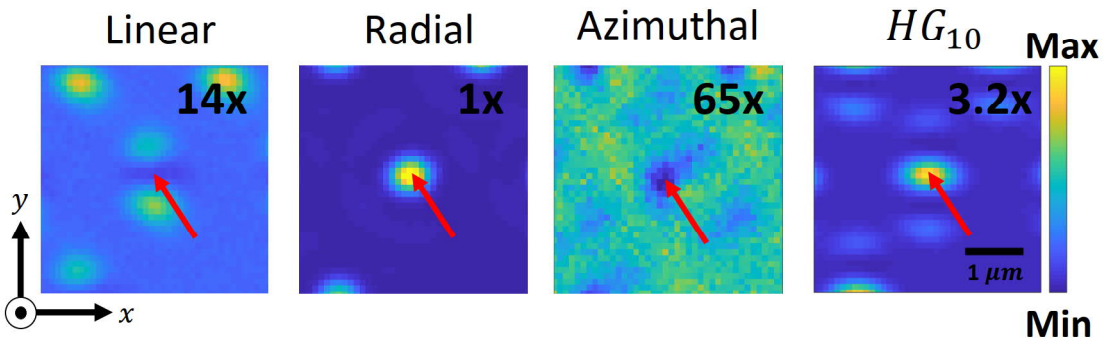

Figure 4.2 *Experimentally verified longitudinal electric field components of the reference beams. The SOPs of LP beam and HG_{10} mode are oriented along the y-axis. The results have been acquired by scanning a single nanowire along the xy-plane. The red arrow shows the location of the nanowire. The colorbar scaling factors have been indicated on the top right-hand corners of the figures.*

Scanning with a radially-polarized CVB creates the strongest SHG signals with a spot-like distribution in the xy-plane. Because the signal is higher, also contrast is much better compared to a scan taken with a LP beam. The scan taken with the azimuthally polarized CVB, on the other hand, has very low signal level. This is because there is no longitudinal electric field at the focus of an azimuthally polarized CVB.

Finally, the nanowires were scanned using a HG_{10} mode. The results show a relatively strong, three-lobed distribution where the middle lobe has the strongest intensity. Similarly as with the LP beam, the orientation of the lobes is determined by the SOP of the input beam.

To verify the longitudinal electric-field distributions in 3D, scans were performed subsequently in yz- and xz-directions. The results are shown in Figures 4.3 and 4.4. In the direction of the z-coordinate, the results show an extended SHG intensity

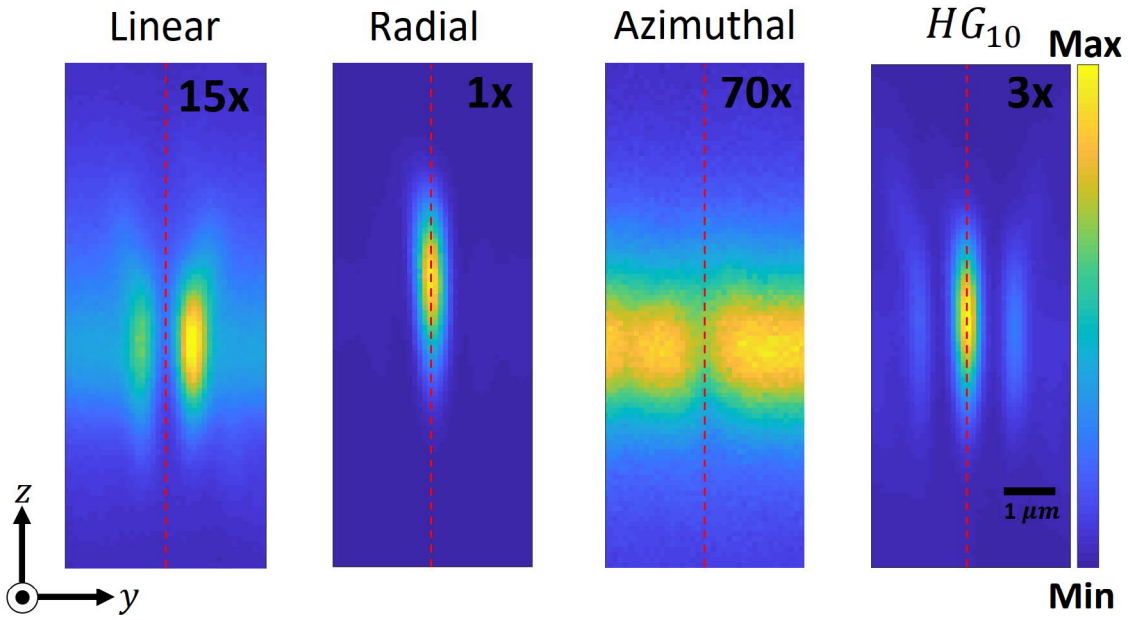

Figure 4.3 *Experimentally verified longitudinal electric field components of the reference beams. The SOPs of LP beam and HG_{10} mode are oriented along y-axis. The results have been acquired by scanning a single nanowire along the yz-plane. The red dashed line shows the location of the nanowire. The colorbar scaling factors have been indicated in the top right corners of the figures.*

distribution with all the used beam profiles. This is a typical characteristic of a point-illumination system because the excitation point spread function is naturally extended along the direction of the beam propagation [28, pp. 19-22]. With all the beams, the signal is the strongest when the beam is focused in the middle of the nanowire. When the beam is not focused on a nanowire, a background signal originating from the sample substrate is generated due to the extensive spread of the focused beam distribution in z-direction.

Scanning the LP beam along the yx-plane, the two-lobed pattern of the focused LP beam can be seen. The xz-scan, on the other hand, shows only a drop in the background signal level at the location of the nanowire. This is because the lobes of the focused LP beam are in the perpendicular direction with respect to the xy-plane. Thus the longitudinal electric field is not hitting the nanowire.

For a radially polarized CVB, the longitudinal scans in the xz- and yz-directions look similar, which can be expected from the symmetrical shape of the longitudinal electric field in the xy-plane. Scanning with an azimuthally polarized CVB results in a very weak SHG signal in both yz- and xz-planes, as there is no longitudinal field.

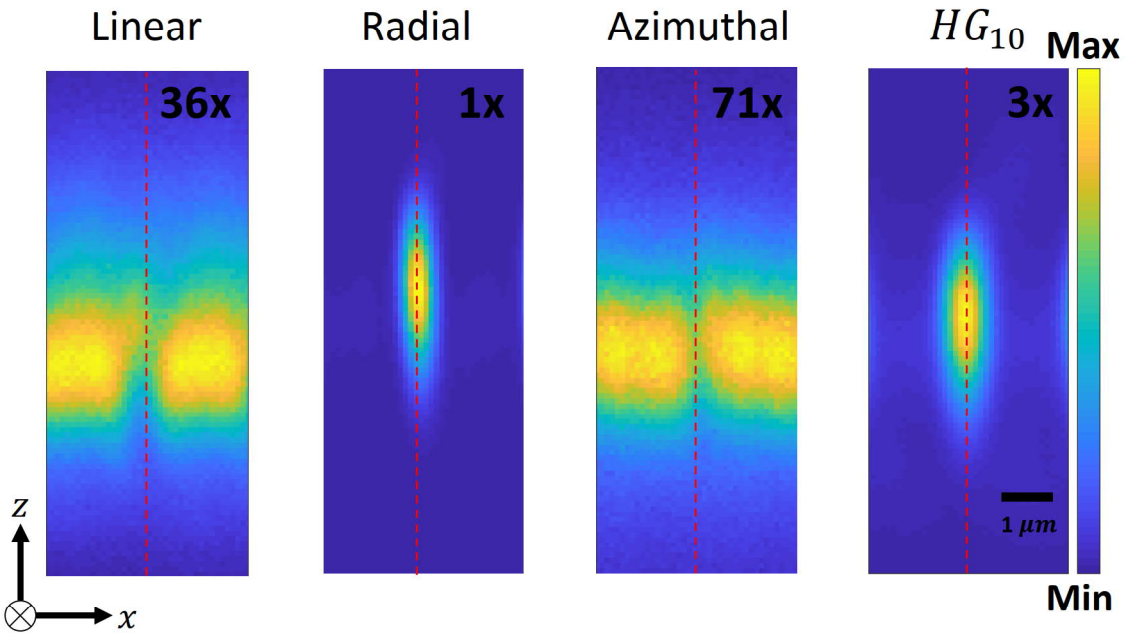

Figure 4.4 *Experimentally verified longitudinal electric field components of the reference beams. The SOPs of LP beam and HG_{10} mode are oriented along y-axis. The results have been acquired by scanning a single nanowire along the xz-plane. The red dashed line shows the location of the nanowire. The colorbar scaling factors have been indicated in the top right corners of the figures.*

Finally, the HG_{10} mode shows a one-lobed distribution in the xz-direction and three-lobed distribution in the yz-direction. The middle lobe shows a wider distribution in the x-direction. These results are expected from the longitudinal electric field distribution of the HG_{10} mode in xy-direction. The work of this thesis was the first time that the longitudinal electric field distribution was experimentally verified for a tightly focused HG_{10} mode.

4.2 Phase-Shaping

After verification of the longitudinal electric field distributions of the reference beam shapes, the SLM was included in the optical setup to perform the phase-shaping experiments described in section 3.2. An additional phase delay was applied to one of the lobes of the HG_{10} mode. The xy-scans with the phase-shaped beams are seen in Figure 4.5.

The scan was taken consequently five times with a different phase delay applied to the beam every time. When the phase delay increases from 0 to π, the longitudinal distribution changes gradually from the three-lobed distribution of HG_{10} mode to

a two-lobed distribution corresponding the one generated by a tightly focused LP beam. On the optical axis, the longitudinal field has vanished to signal level corresponding background. As the phase delay increases to 2π, the distribution converts back to the original. These results are similar to the results of Turquet et al. [15].

The result is expected as when the phase of the other lobe is delayed by π, the electric field in the two lobes oscillates in the same phase, which make the resulting beam to be equivalent to a LP beam. On the other hand, the delay of 2π should make no difference to the original.

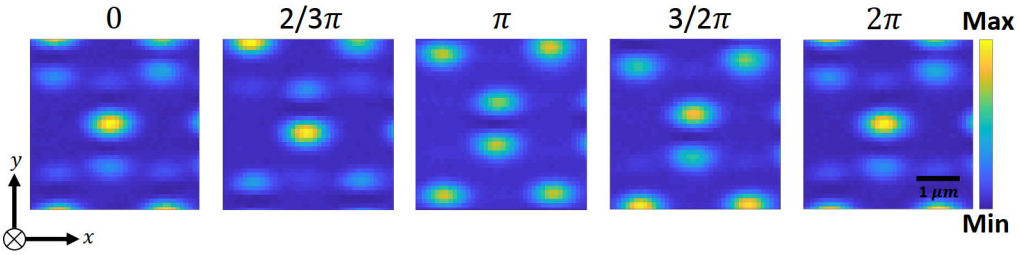

Figure 4.5 *Experimentally verified longitudinal electric field components of the phase-shaped beams. The results have been acquired by scanning a single nanowire along the xy-plane.*

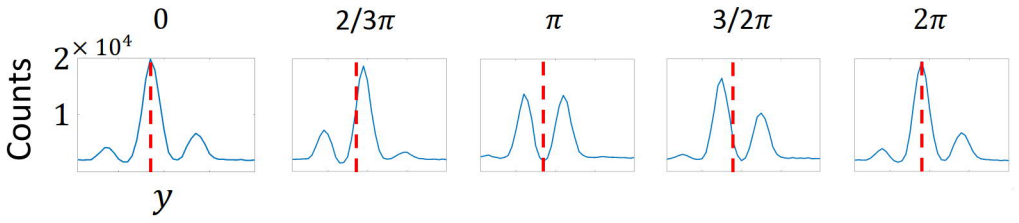

Figure 4.6 *Linecuts taken along the y-axis from figure 4.5. The location of the nanowire is marked with a red dashed line.*

In Figure 4.6, linecuts taken along the y-axis of the results in Figure 4.5 are shown. The linecuts show that the maximum signal level drops to little over half when the phase delay is π. From the law of energy conservation, one can expect that the missing intensity has now transferred to transverse polarization components. This is also supported by the theoretically and experimentally verified 3D field distributions of LP beam and HG_{10} mode.

In Figure 4.7, the nanowires are imaged along the yz-plane. Figure 4.8 shows linecuts taken along y-axis of Figure 4.7. The data of Figures 4.6 and 4.8 look very similar, which indicates that our probing has been successful.

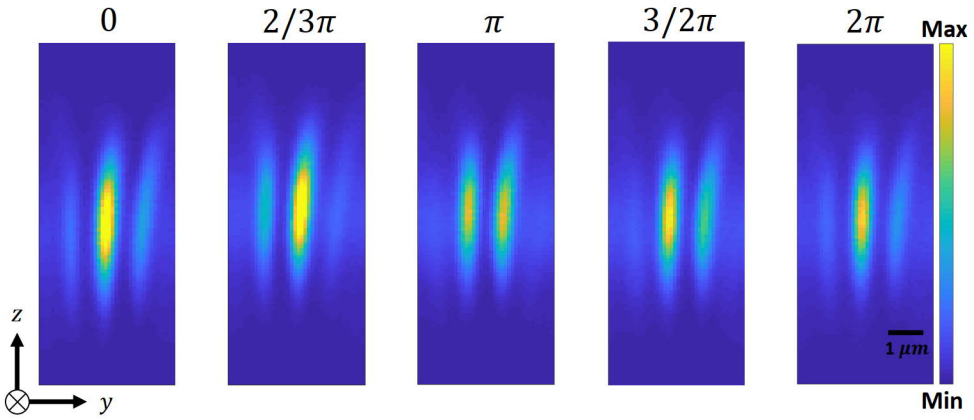

Figure 4.7 *Experimentally verified longitudinal electric field components of the phase-shaped beams. The results have been acquired by scanning a single nanowire along the yz-plane.*

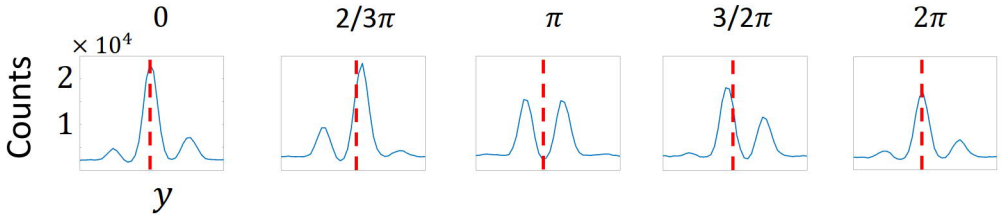

Figure 4.8 *Linecuts taken along the y-axis from figure 4.7. The location of the nanowire is marked with a red dashed line.*

The results confirm the phase shaping results to be similar also in 3D compared to the results of earlier phase shaping experiments in transverse plane, for instance in Ref. [15]. In the work of this thesis, it was the first time that a spatially phase shaped higher order beam was mapped in three dimensions using this kind of method. Comparing to the results of reference beams, the distribution is also extended along the z-coordinate. This phase shaping experiment gave us a new way to synthesize and directly probe longitudinal electric fields in three dimensions.

Being able to control and probe the distribution of different polarization components is very important in controlling light-matter interactions. These results show that, by phase shaping the incident beam entering the microscope objective, the longitudinal electric field distribution in the focus of the beam can be controlled. The results imply, for example, that with this kind of setup the longitudinal electric field on the optical axis can be quickly turned on and off without cumbersomely modifying the alignment of the beam or the physical components on the optical path.

5. CONCLUSIONS AND OUTLOOK

Polarization is a very important property of light. For example generation of nonlinear effects, such as SHG, are highly dependent on the polarization of the light field [2]. It is also known that highly focused light creates a 3D polarization distribution, which can be probed with nanostructures. This is particularly useful in NLO microscopy to study nanoparticles as well as biological samples. In this context, it is crucial to be able to tailor the polarization components at the beam focus in order to maximize image contrast or manipulate the efficiency of light-matter interactions at the nanoscale.

In this Thesis, we presented a method to manipulate the longitudinal electric field distribution of a tightly focused higher-order beam. The control was achieved using a spatial light modulator, which allowed us to arbitrarily adjust the relative phase difference of the lobes of HG_{10} mode. The phase shaping scheme presented in this Thesis allowed us to redistribute the longitudinal electric field in transverse plane. We were also able to reliably verify the generated field distribution in 3D by using semiconductor nanowires. In previous experiments of Turquet et al. [15], the redistributed field was verified in transverse plane, but in this work, we mapped the SHG generation also in vertical plane to verify the field distribution in 3D.

This work provided a new blueprint to tailor beam polarization for NLO microscopy and other applications as well. However, there is still room for improvement towards even more arbitrary control. For example, extension of the field distribution in the longitudinal direction can already be controlled with optical needles [26]. Among the distribution of the field, also the 3D location of the generated fields could be controlled with more sophisticated phase-shaping methods. The methods presented in this work lacks a way to verify the transverse field components at the beam focus. We foresee that this could be mitigated by the combination of our imaging technique and advanced nanostructures with fully tailorable second-order susceptibilities. This is a subject of future work.

BIBLIOGRAPHY

[1] R. Boyd, *Nonlinear Optics*, 3rd ed. Academic Press, 2007.

[2] G. Bautista and M. Kauranen, "Vector-field nonlinear microscopy of nanostructures," *ACS Photonics*, vol. 3, no. 8, pp. 1351–1370, 2016. [Online]. Available: https://doi.org/10.1021/acsphotonics.6b00052

[3] D. Yelin and Y. Silberberg, "Laser scanning third-harmonic-generation microscopy in biology," *Opt. Express*, vol. 5, no. 8, pp. 169–175, 10 1999. [Online]. Available: http://www.opticsexpress.org/abstract.cfm?URI=oe-5-8-169

[4] P. J. Campagnola, M. de Wei, A. Lewis, and L. M. Loew, "High-resolution nonlinear optical imaging of live cells by second harmonic generation," *Biophysical Journal*, vol. 77, no. 6, pp. 3341 – 3349, 1999. [Online]. Available: http://www.sciencedirect.com/science/article/pii/S0006349599771651

[5] O. Nadiarnykh, R. B. LaComb, M. A. Brewer, and P. J. Campagnola, "Alterations of the extracellular matrix in ovarian cancer studied by second harmonic generation imaging microscopy," *BMC Cancer*, vol. 10, no. 1, p. 94, 3 2010. [Online]. Available: https://doi.org/10.1186/1471-2407-10-94

[6] B. Richards and E. Wolf, "Electromagnetic diffraction in optical systems, ii. structure of the image field in an aplanatic system," *Proceedings of the Royal Society of London A: Mathematical, Physical and Engineering Sciences*, vol. 253, no. 1274, pp. 358–379, 1959. [Online]. Available: http://rspa.royalsocietypublishing.org/content/253/1274/358

[7] K. Lindfors, A. Priimagi, T. Setälä, A. Shevchenko, A. T. Friberg, and M. Kaivola, "Local polarization of tightly focused unpolarized light," *Nature Photonics*, vol. 1, no. 1, pp. 228–231, 4 2007. [Online]. Available: http://dx.doi.org/10.1038/nphoton.2007.30

[8] G. Bautista, J. Mäkitalo, Y. Chen, V. Dhaka, M. Grasso, L. Karvonen, H. Jiang, M. J. Huttunen, T. Huhtio, H. Lipsanen, and M. Kauranen, "Second-harmonic generation imaging of semiconductor nanowires with focused vector beams," *Nano Letters*, vol. 15, no. 3, pp. 1564–1569, 2015, pMID: 25651302. [Online]. Available: https://doi.org/10.1021/nl503984b

[9] Q. Zhan, "Cylindrical vector beams: from mathematical concepts to applications," *Adv. Opt. Photon.*, vol. 1, no. 1, pp. 1–57, 1 2009. [Online]. Available: http://aop.osa.org/abstract.cfm?URI=aop-1-1-1

[10] O. Svelto, *Principles of Lasers*, 5th ed. Springer, 2010, 620 p.

[11] L. Novotny, E. J. Sánchez, and X. S. Xie, "Near-field optical imaging using metal tips illuminated by higher-order hermite-gaussian beams," *Ultramicroscopy*, vol. 71, no. 1, pp. 21 – 29, 1998. [Online]. Available: http://www.sciencedirect.com/science/article/pii/S0304399197000776

[12] Y. I. Salamin and C. H. Keitel, "Electron acceleration by a tightly focused laser beam," *Phys. Rev. Lett.*, vol. 88, p. 095005, 2 2002. [Online]. Available: https://link.aps.org/doi/10.1103/PhysRevLett.88.095005

[13] Y. I. Salamin, G. R. Mocken, and C. H. Keitel, "Electron scattering and acceleration by a tightly focused laser beam," *Phys. Rev. ST Accel. Beams*, vol. 5, p. 101301, 10 2002. [Online]. Available: https://link.aps.org/doi/10.1103/PhysRevSTAB.5.101301

[14] Y. Zhao, J. S. Edgar, G. D. M. Jeffries, D. McGloin, and D. T. Chiu, "Spin-to-orbital angular momentum conversion in a strongly focused optical beam," *Phys. Rev. Lett.*, vol. 99, p. 073901, 8 2007. [Online]. Available: https://link.aps.org/doi/10.1103/PhysRevLett.99.073901

[15] L. Turquet, J.-P. Kakko, X. Zang, L. Naskali, L. Karvonen, H. Jiang, T. Huhtio, E. Kauppinen, H. Lipsanen, M. Kauranen, and G. Bautista, "Tailorable second-harmonic generation from an individual nanowire using spatially phase-shaped beams," *Laser & Photonics Reviews*, vol. 11, no. 1, p. 1600175, 2016. [Online]. Available: https://onlinelibrary.wiley.com/doi/abs/10.1002/lpor.201600175

[16] E. Y. S. Yew and C. J. R. Sheppard, "Effects of axial field components on second harmonic generation microscopy," *Opt. Express*, vol. 14, no. 3, pp. 1167–1174, 2 2006. [Online]. Available: http://www.opticsexpress.org/abstract.cfm?URI=oe-14-3-1167

[17] R. Cisek, V. Barzda, H. E. Ruda, and A. Shik, "Nonlinear optical properties of semiconductor nanowires," *IEEE Journal of Selected Topics in Quantum Electronics*, vol. 17, no. 4, pp. 915–921, 7 2011.

[18] G. Bautista, J.-P. Kakko, V. Dhaka, X. Zang, L. Karvonen, H. Jiang, E. Kauppinen, H. Lipsanen, and M. Kauranen, "Nonlinear microscopy using cylindrical vector beams: Applications to three-dimensional imaging

of nanostructures," *Opt. Express*, vol. 25, no. 11, pp. 12 463–12 468, 5 2017. [Online]. Available: http://www.opticsexpress.org/abstract.cfm?URI=oe-25-11-12463

[19] C. Maurer, A. Jesacher, S. Fürhapter, S. Bernet, and M. Ritsch-Marte, "Tailoring of arbitrary optical vector beams," *New J. Phys.*, vol. 9, no. 78, 3 2007. [Online]. Available: http://iopscience.iop.org/article/10.1088/1367-2630/9/3/078

[20] M. Bashkansky, D. Park, and F. K. Fatemi, "Azimuthally and radially polarized light with a nematic slm," *Opt. Express*, vol. 18, no. 1, pp. 212–217, 1 2010. [Online]. Available: http://www.opticsexpress.org/abstract.cfm?URI=oe-18-1-212

[21] X.-L. Wang, J. Ding, W.-J. Ni, C.-S. Guo, and H.-T. Wang, "Generation of arbitrary vector beams with a spatial light modulator and a common path interferometric arrangement," *Opt. Lett.*, vol. 32, no. 24, pp. 3549–3551, 12 2007. [Online]. Available: http://ol.osa.org/abstract.cfm?URI=ol-32-24-3549

[22] J. Leach, K. Wulff, G. Sinclair, P. Jordan, J. Courtial, L. Thomson, G. Gibson, K. Karunwi, J. Cooper, Z. J. Laczik, and M. Padgett, "Interactive approach to optical tweezers control," *Appl. Opt.*, vol. 45, no. 5, pp. 897–903, 2 2006. [Online]. Available: http://ao.osa.org/abstract.cfm?URI=ao-45-5-897

[23] A. Jesacher, C. Maurer, A. Schwaighofer, S. Bernet, and M. Ritsch-Marte, "Near-perfect hologram reconstruction with a spatial light modulator," *Opt. Express*, vol. 16, no. 4, pp. 2597–2603, 2 2008. [Online]. Available: http://www.opticsexpress.org/abstract.cfm?URI=oe-16-4-2597

[24] L. Turquet, J.-P. Kakko, H. Jiang, T. J. Isotalo, T. Huhtio, T. Niemi, E. Kauppinen, H. Lipsanen, M. Kauranen, and G. Bautista, "Nonlinear imaging of nanostructures using beams with binary phase modulation," *Opt. Express*, vol. 25, no. 9, pp. 10 441–10 448, 5 2017. [Online]. Available: http://www.opticsexpress.org/abstract.cfm?URI=oe-25-9-10441

[25] L. Turquet, J.-P. Kakko, L. Karvonen, H. Jiang, E. Kauppinen, H. Lipsanen, M. Kauranen, and G. Bautista, "Probing the longitudinal electric field of bessel beams using second-harmonic generation from nano-objects," *Journal of Optics*, vol. 19, no. 8, p. 084011, 7 2017. [Online]. Available: https://doi.org/10.1088%2F2040-8986%2Faa7722

[26] L. Turquet, X. Zang, J.-P. Kakko, H. Lipsanen, G. Bautista, and M. Kauranen, "Demonstration of longitudinally polarized optical needles,"

Opt. Express, vol. 26, no. 21, pp. 27 572–27 584, 10 2018. [Online]. Available: http://www.opticsexpress.org/abstract.cfm?URI=oe-26-21-27572

[27] L. Turquet, "Manipulation and verification of longitudinal electric fields for nonlinear optical microscopy," Ph.D. dissertation, Tampere University of Technology, 2018.

[28] T. Wilson and C. Sheppard, *Theory And Practice Of Scanning Optical Microscopy*. London: Academic Press, 10 1984.